Surv Geophys (2013) 34:521–529
DOI 10.1007/s10712-013-9228-0

Comment on the Seismic Method Depth-Recursive Tomography on Grid (DRTG) Developed by Miroslav Novotný and Recently Published in Three Papers in *Surveys in Geophysics*

Pavla Hrubcová · Piotr Środa · Václav Vavryčuk · Vladislav Babuška · Marek Grad

Received: 14 June 2012 / Accepted: 22 March 2013 / Published online: 4 April 2013

The comment addresses three papers published recently in Surveys in Geophysics. These papers are related, using the same seismic tomography approach developed by the same first author. They deal with modelling of seismic refraction crustal data in the Bohemian Massif and their geological interpretation. Novotný (2011) presents a *P*-wave velocity model based on tomography along the refraction profile CEL09 of the CELEBRATION 2000 experiment; Novotný (2012) presents a geological interpretation of this model. Novotný et al. (2009) interpret a part of the S01 seismic refraction profile of the SUDETES 2003 experiment and present both a seismic velocity model and a detailed geological model derived from it.

All results in the three mentioned papers are obtained using a seismic method, developed by the first author, called the Depth-Recursive Tomography on Grid (DRTG). This method is based on a regular network of refraction grid rays generated for iteratively updated models. Though data and shot points of both experiments are not equidistantly spaced along the profiles, the DRTG method employs a regular system of refraction rays

Papers of the Comment
Depth-Recursive Tomography Along the Eger Rift Using the S01 Profile Refraction Data: Tested at the KTB Super Drilling Hole, Structural Interpretation Supported by Magnetic, Gravity and Petrophysical Data, Miroslav Novotný, Zuzana Skácelová, Jan Mrlina, Bedřich Mlčoch and Bohuslav Růžek, Surv Geophys 30(6):561–600. doi:10.1007/s10712-009-9068-0, 2009.
Depth-Recursive Tomography of the Bohemian Massif at the CEL09 Transect—Part A: Resolution Estimates and Deblurring Aspects, Miroslav Novotný, Surv Geophys 32(6):827–855. doi:10.1007/s10712-011-9143-1, 2011.
Depth-Recursive Tomography of the Bohemian Massif at the CEL09 Transect—Part B: Interpretation, Miroslav Novotný, Surv Geophys 33(2):243–273. doi:10.1007/s10712-011-9155-x, 2012.

P. Hrubcová (✉) · V. Vavryčuk · V. Babuška
Institute of Geophysics, Academy of Sciences, Boční II/1401, 141 31 Prague 4, Czech Republic
e-mail: pavla@ig.cas.cz

P. Środa
Institute of Geophysics, Polish Academy of Sciences, Ks. Janusza 64, 01-452 Warsaw, Poland

M. Grad
Faculty of Physics, Institute of Geophysics, University of Warsaw, Pasteura 7, 02-093 Warsaw, Poland

that uniformly covers the mapped domain. According to the authors, only the first *Pg* arrivals are used in the modelling process, and the authors apply some control of the data fit by the grid rays. When the DRTG tomography is applied, the *P*-wave velocity models along both profiles are obtained down to a depth of 20 km. Special attention is paid to the imaging of low-velocity zones usually suppressed by smoothing in standard tomographic methods. The resulting fine-grid velocity models are interpreted to produce detailed geological models.

In this comment, we would like to point out essential deficiencies of the DRTG tomography approach that lead to seismic velocity models and consequently to detailed geological interpretations not constrained by the data. To document this, we performed three synthetic tests with one of the discussed models presented by Novotný (2011, Figure 10), the CEL09 model, in order to evaluate its quality and resolution.

1 Refraction Data in the Bohemian Massif

The area of interest, the Bohemian Massif with metamorphic/crystalline rocks exposed at the surface and at most with a thin sedimentary cover, is characterized by a high-velocity gradient in the uppermost crust followed by a low (sometimes close to zero)-velocity gradient in the upper/middle crust (Hrubcová et al. 2005; Růžek et al. 2007; Hrubcová et al. 2008; Hrubcová et al. 2010). The low gradient in the upper/middle crust is also evidenced by a relatively fast decrease of *Pg* amplitude visible in seismic sections of the refraction experiments (e.g., Hrubcová et al. 2005; Grad et al. 2008). For such a gradient, even the deepest Pg rays, recorded at offsets typical for this method, bottom at shallow crustal depths. Assuming a realistic, low gradient in the middle crust based on the observed *Pg* traveltimes and amplitudes, we can expect the penetration depth of the most of the *Pg* rays in the first arrivals to be no more than about 5–10 km below surface depending on the actual *Vp* (e.g., Hrubcová et al. 2010, Figure 4, left side, green line). Therefore, an inversion method which uses only the *Pg* wave in the first arrivals is not, in principle, able to recover velocities in deeper parts of the crust in this area.

A theoretical example of such a case is presented by Zelt (1999), who shows a depth dependence of wide-angle seismic rays in a typical crust. In this example, refracted rays corresponding to traveltimes of the *Pg* first arrivals constrain the upper crust down to $\sim$10 km only. In the absence of other, higher velocity crustal refracted phases (or reflected arrivals) the deeper parts of the crust remain unconstrained. Apart from arrival times, additional constraint on the velocity in deeper crust can be given by amplitude modelling. The amplitude assessment is especially necessary when introducing low-velocity zones. Neither of these constraints is applied in the DRTG tomography models, which are only based on the inversion of the first-arrival *Pg* traveltimes.

2 Interpolation/Extrapolation of the Data Set

The DRTG inversion used by the authors requires special processing of the data to create a regularly spaced traveltime field in the offset/midpoint domain t(p,q). The picked traveltimes, irregularly spaced and with several gaps, were first resampled in the offset domain along individual traveltime curves to equidistant positions with 2 or 3 km step. Thus, the

gaps in real data, sometimes large (~20 km; e.g., Novotný 2011, Figure 4, SP 29040, right branch), were filled by interpolated traveltimes. However, they are not the actual traveltime data. According to the authors, in the next step, these interpolated traveltimes were sorted into the common offset sets. Then, the traveltimes in each such a set were interpolated in the midpoint domain to produce the 'time lines' (e.g., Novotný 2011, Figure 4) with a midpoint step of 5 km. In this way, interpolated t(p,q) set consisted of over 4,000 points compared to ~1,000 real (picked) data points. Using this procedure, not only the amount of data was increased (equivalent to interpolation), but also traveltime curves were extended to higher times (equivalent to extrapolation towards large offsets) and supplemented with traveltime points interpolated between neighbouring shot points, (e.g., Novotný et al. 2009, Figure 4, the traveltime curves above 15 s for at least the 4th, 8th, and 9th shot points, left branches, numbered from left side).

Since the shot points are located quite far (~30–100 km from each other), the real sampling interval of the time lines in the midpoint domain is quite large (tens of km). Thus, the determination of a missing part of the traveltime curve (i.e. extrapolation up to the maximum traveltime used for the inversion) based on traveltimes from distant shot points requires an assumption of laterally uniform structure over large areas, especially in deeper parts of the models. Mathematically, such an interpolation is possible, and its effect is similar to smoothing applied during an inversion to stabilize unconstrained parts of the model. However, in discussed papers, the density of the real data set with gaps and missing parts in higher traveltimes is far from such an interpolated data set. Thus, the distribution of rays and their bottoming points for interpolated data (presented in Novotný 2011, Figure 7) does not reflect the real data and the true ray coverage.

Another related problem is the fact that the traveltimes in Novotný (2011, Figure 4) reach over 30 s, which is beyond the cross-over point of the *Pg* and *Pn* phase in the Bohemian Massif, especially in its middle part. Therefore, these data cannot be the *Pg* in the first arrivals but according to the apparent velocities they represent the *Pn* phase. Since the *Pn* phase brings information about the velocity in the upper mantle, interpolation/extrapolation between crustal and upper mantle data imposes unrealistic anomalies in deeper parts of the models.

To document the actual data coverage of published models that can be obtained with the real data used by the authors, we performed a test involving ray tracing and travel time calculation with the finite-difference code by Vidale (1990) (Fig. 1). The CEL09 model presented by Novotný (2011, Figure 10) was digitized, as well as corresponding travel time picks (Novotný 2011, Figure 4, red crosses). The ray tracing calculation through this model for picked data points showed that the ray density decreases abruptly (by about 5 times, Fig. 1a) at a depth below 8 km, resulting in low and non-uniform ray coverage in deeper parts, leaving large parts of the model unconstrained. The test clearly shows that for the picked CEL09 data set, the distribution of the bottoming points of the successful rays is dramatically different and much worse than presented by Novotný (2011, Figure 7) as visible when comparing Fig. 1b, c, d with e. Therefore, Figure 7 of Novotný (2011) is not a correct measure of the ray coverage. On the contrary, the evaluation of the model reliability should have been done only for the points corresponding to the picked traveltimes (thus representing the real data constraints); otherwise it imposes the impression of higher than realistic constraints. It should be stressed that the distribution of rays for given geometry of source-receiver pairs only depends on the velocities in the medium and not on the forward or the inversion method used. Thus, the DRTG method cannot produce successful rays in places where they are not present in reality.

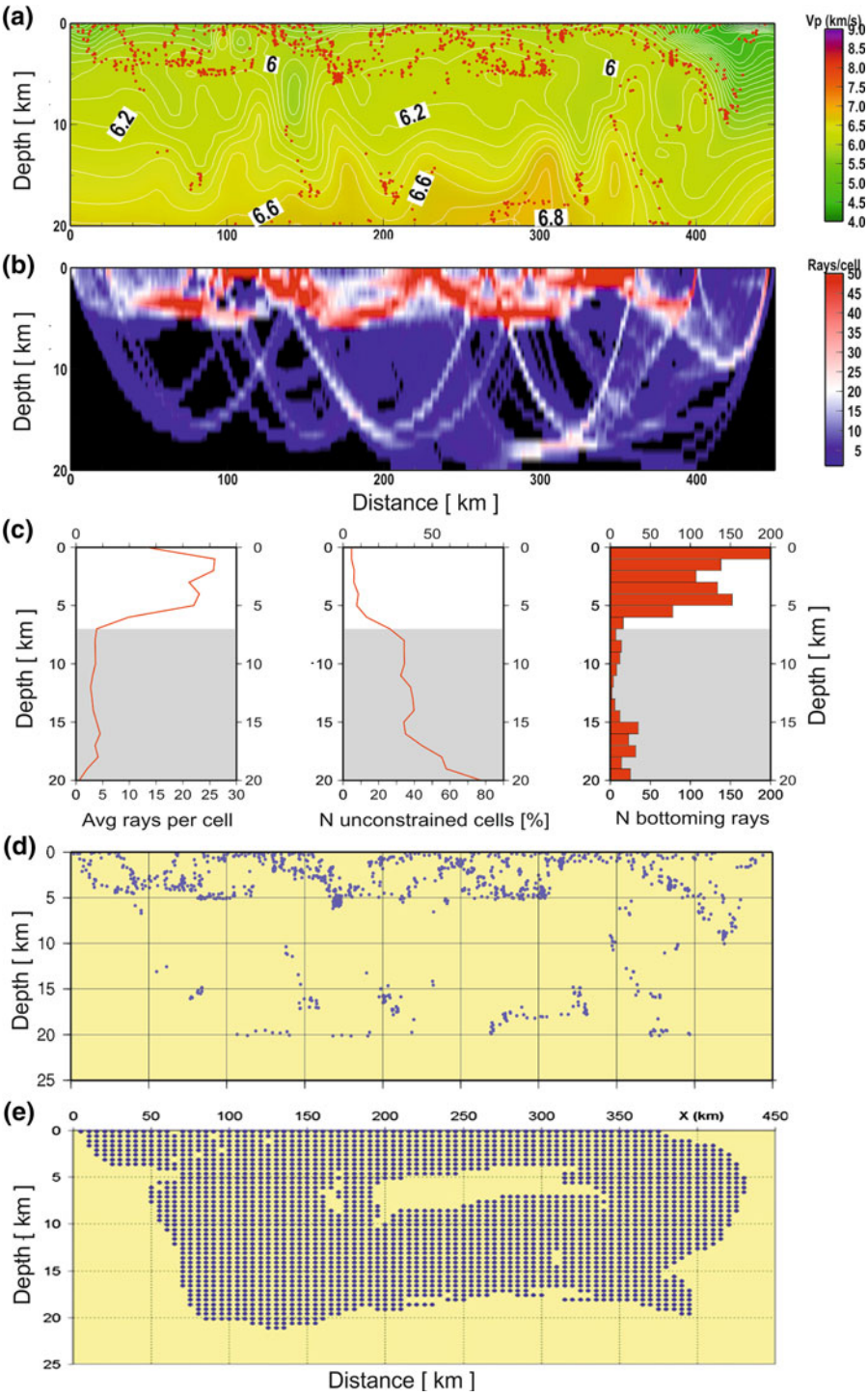
(a)
Depth [km]
Vp (km/s)
6
6.2
6.6
6.8
(b)
Depth [km]
Rays/cell
Distance [km]
(c)
Depth [km]
Avg rays per cell
N unconstrained cells [%]
N bottoming rays
(d)
Depth [km]
(e)
Depth [km]
X (km)
Distance [km]

◀ **Fig. 1** Ray tracing for CEL09 model of Novotný (2011, Figure 10). **a** The digitized CEL09 model. *Red dots* show locations of bottoming points of successful rays. **b** Results of the finite-difference ray tracing for the digitized CEL09 model and for the source-receiver geometry corresponding to picked traveltimes. **c** Diagrams of average ray density at given depth; percentage of unconstrained cells; number of bottoming rays. *Grey rectangle* highlights the depth interval with an abrupt decrease in the ray coverage. **d** Bottoming points of successful grid rays for the digitized CEL09 model. **e** Bottoming points of successful grid rays presented by Novotný (2011, Figure 7). Note the vast difference in the distribution of the bottoming points of calculated rays compared to the one of Novotný (2011, Figure 7)

3 Periodic Velocity Anomalies at Mid-Crustal Depths

The S01 and CEL09 seismic models from DRTG tomography are modelled and interpreted in the form of *P*-velocity isolines down to depths of 15 km (profile S01, Novotný et al. 2009, Figure 9) and 20 km (profile CEL09, Novotný 2011, Figure 10). The lower parts of these models show high and low lateral velocity oscillations. The laterally oscillating isolines of high and low velocities in the lower parts of both models are in a depth range of 10–20 km and correspond with the high positive and negative velocity residuals oscillating in a similar way (e.g., Novotný et al. 2009, Figure 9d). This suggest either a lack of or insufficient constraints at deeper parts of the models. The authors interpret these regularly repeated velocity anomalies in the middle crust (at $\sim$15 km depths) in terms of real geological features, deep faults, and contacts of different units at depth.

To document insufficient constraints on the deeper velocity anomalies, we performed the second test (Fig. 2). This test showed that the published CEL09 model (Novotný 2011, Figure 10) and the same model with horizontally averaged 1-D velocity structure at depths in range of 8–20 km exhibit the same RMS residual values ($\sim$0.18 s, which is even slightly lower than the RMS for the published CEL09 model of 0.19 s). Since the traveltime residuals as the main measure of the model quality did not change significantly after replacing the published CEL09 model (Novotný 2011, Figure 10) with a simpler 1-D model, the velocity anomalies in deeper crustal parts are not needed to fit the experimental traveltime data.

The third test involved ray tracing for the published CEL09 model with the part at 9–20 km depth laterally shifted in a range of -100 to $+100$ km, with a step of 20 km. The results of this test disclosed that the strong velocity anomalies modelled by Novotný (2011, Figure 10) at depths below 9 km can be horizontally shifted by as much as $\sim$80 km without a significant increase in the RMS residuals (Fig. 3). From this test, it is clear that high-velocity anomalies can roughly be replaced by low-velocity anomalies (and vice versa), still preserving the same fit to the traveltime data as for the original model. Thus, the test shows insufficient constraint imposed by the sparse ray coverage at a depth of 9–20 km.

Both tests documented in Figs. 2, 3 denote that the velocity anomalies at depths of 9–20 km modelled by Novotný (2011, Figure 10) are not realistic, since models with different velocity structures are equally possible. Thus, these parts of the models cannot be considered for any geological/tectonic interpretation.

It should be stressed that the model of Novotný (2011, Figure 10) and presented alternative models represent mathematically equal solutions in terms of data fit (RMS residuals). However, analysis of the true ray coverage provides the simplest criterion to determine which parts of the model are robust. That is the reason why such an analysis is important and is required during any modelling. Thus, the parts of the model without reliable constraints should be interpreted in terms of the simplest (minimum-structure)

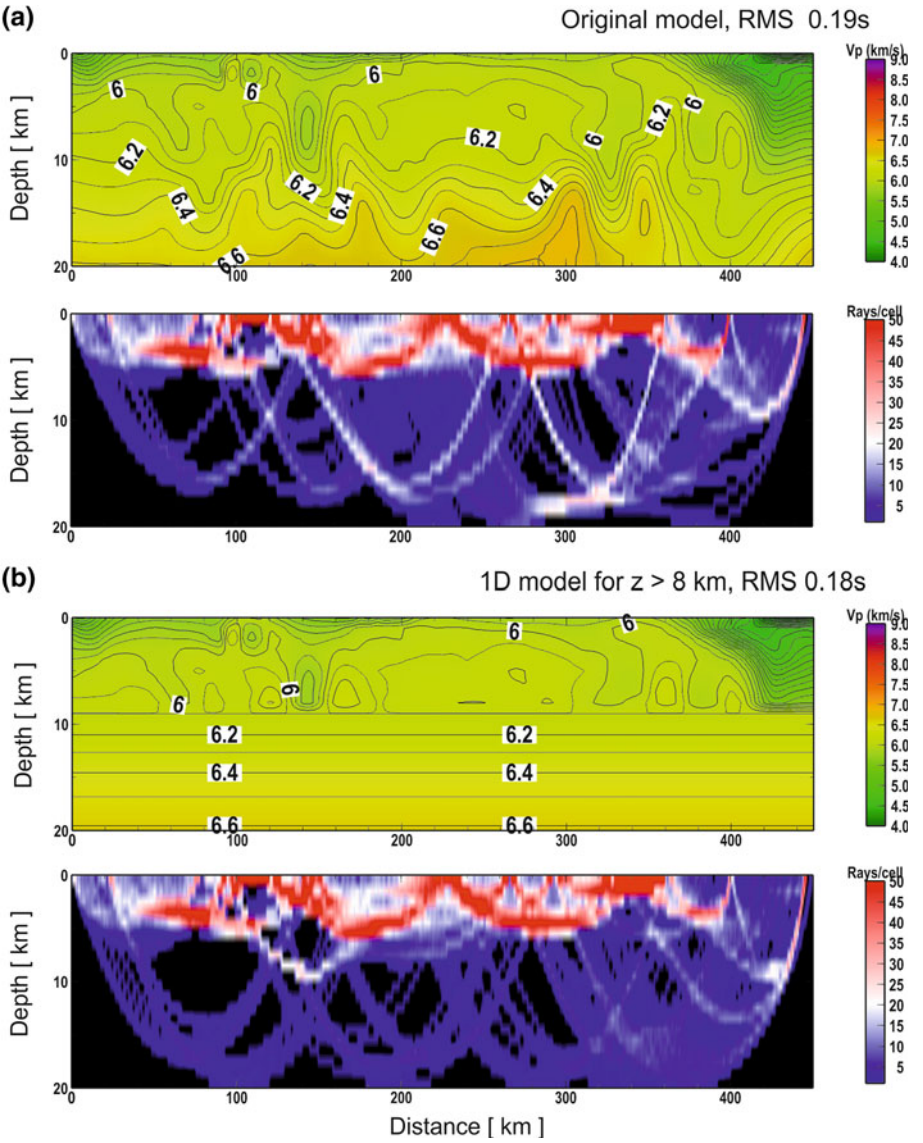

Fig. 2 **a** CEL09 velocity model of Novotný (2011, Figure 10), and **b** this model replaced by a 1-D velocity distribution below 8 km depth. Both models have corresponding ray coverage. Note comparable RMS residuals for both models (0.19 s for the original model and 0.18 s for the model with 1-D below 8 km depth)

solution which still fits the experimental data, or they should be excluded from further interpretation. Though the published CEL09 and S01 models (Novotný 2011; Novotný et al. 2009) provided analysis of the respective ray coverage, their evaluation of constraints was based on an incorrect (overestimated) image of the density of the rays and their bottoming points (as disclosed above). For these reasons, the assessment of the quality of these models was not correct.

4 Geological Interpretations of Unconstrained Velocity Models

The geological interpretations, though based on unconstrained seismic DRTG tomography models, are very detailed. Disregarding high alternating velocity residuals (e.g., Novotný et al. 2009, Figure 9d), the authors correlate strong seismic anomalies in deeper crustal parts to depths of ~20 km (profile CEL09, Novotný 2011) or to depths of ~15 km (profile S01, Novotný et al. 2009) with surface geology. Since the velocity anomalies are not constrained by the data, this can imply tectonic conclusions that are not well founded. The geological cross-section of Novotný et al. (2009, Figure 14c) is too detailed to be resolved by the seismic data. The same applies to correlation of deep-seated near-vertical faults with velocity anomalies from DTRG tomography (see, e.g., the Blanice Rodl Fault in Novotný 2012, Figure 1). Thus, the seismic DRTG tomography modelling can lead to over-interpretation/misinterpretation of the presented *P*-velocity isolines.

The authors claim that the *P*-velocity depicted in the Figure 14b (Novotný et al. 2009) reflects the subsurface geology in the most direct way if compared with previously discussed 'geopotential data' (p. 587) and they contour geological bodies in Figure 14c according to the *P*-velocity isolines. In their view, the isolines of velocity of 6.1 km/s delimit occurrences of ultrabasic rocks (bodies 7 and 13). They also assume that 'the granitic bodies are distinguished very well with their lower densities and velocities (up to ~5.9 km/s)'. In reality, the ultrabasic rocks have *P* velocities ~8 km/s, or more (e.g., Babuška and Cara 1991), unless these rocks are serpentinized, but the authors do not mention any secondary changes. Similarly, the authors contour a 'basement' by the unreliably produced isolines of ~6.2–6.3 km/s at depths of 10–15 km but they do not explain the meaning of this term. The term is usually used in geology of sedimentary basins as a crystalline basement beneath sediments. Besides the problematic course of the *P*-velocity isolines, there are overlapping extents of *P* velocities in individual rock types (Novotný et al. 2009, Table 5). Moreover, the authors do not state under which laboratory conditions (e.g., a pressure at a corresponding depth) the velocities in rock samples were measured. This makes their geological interpretations even more questionable.

Novotný (2012) focuses on the interpretation of the CEL09 profile. Among several other problematic statements, they suggest that the 'transect reveals seven major deeply rooted high-velocity (HV) anomalies identified as Variscan massifs intruded near or within the deep fault zones' (Novotný 2012, Abstract). In reality, these 'diapiric mafic intrusions' (the term 'Variscan massifs' should not be used in this context) most probably do not exist at all. Figure 1 in Novotný (2012) images 'mass flow vectors' that point downwards in the case of low-velocity anomalies, indicating thus a transfer of a low-density material from upper to deeper crustal levels. On the other hand, the upwellings of unreliably determined isolines of *P* velocities between ~6.3 and 6.8 km/s at depths between 10 and 20 km are interpreted as 'mafic intrusions'. Actually, all mass displacements in the Earth are a result of gravitational forces, as a gravity-driven flow tends to reduce lateral contrasts in gravitational potential energy (e.g., Rey et al. 2001). But the 'mass flow vectors' in Figure 1 (Novotný 2012) are oriented in the opposite directions. Similarly, it is difficult to imagine the ultrabasic massifs (Nos. 7 and 12 in Figure 14, Novotný et al. 2009) with dimensions of ~30–60 km at depths of 5–12 km. It is generally accepted that high-density mantle rocks need 'an elevator' of deeply subducted low-density crustal rocks like granites that are able to exhume captured pieces of the mantle in the upper crust (e.g., Ernst et al. 1997). But neither the dimensions nor the tectonic position of the ultrabasic bodies in Figure 14 (Novotný et al. 2009) permit such a scenario.

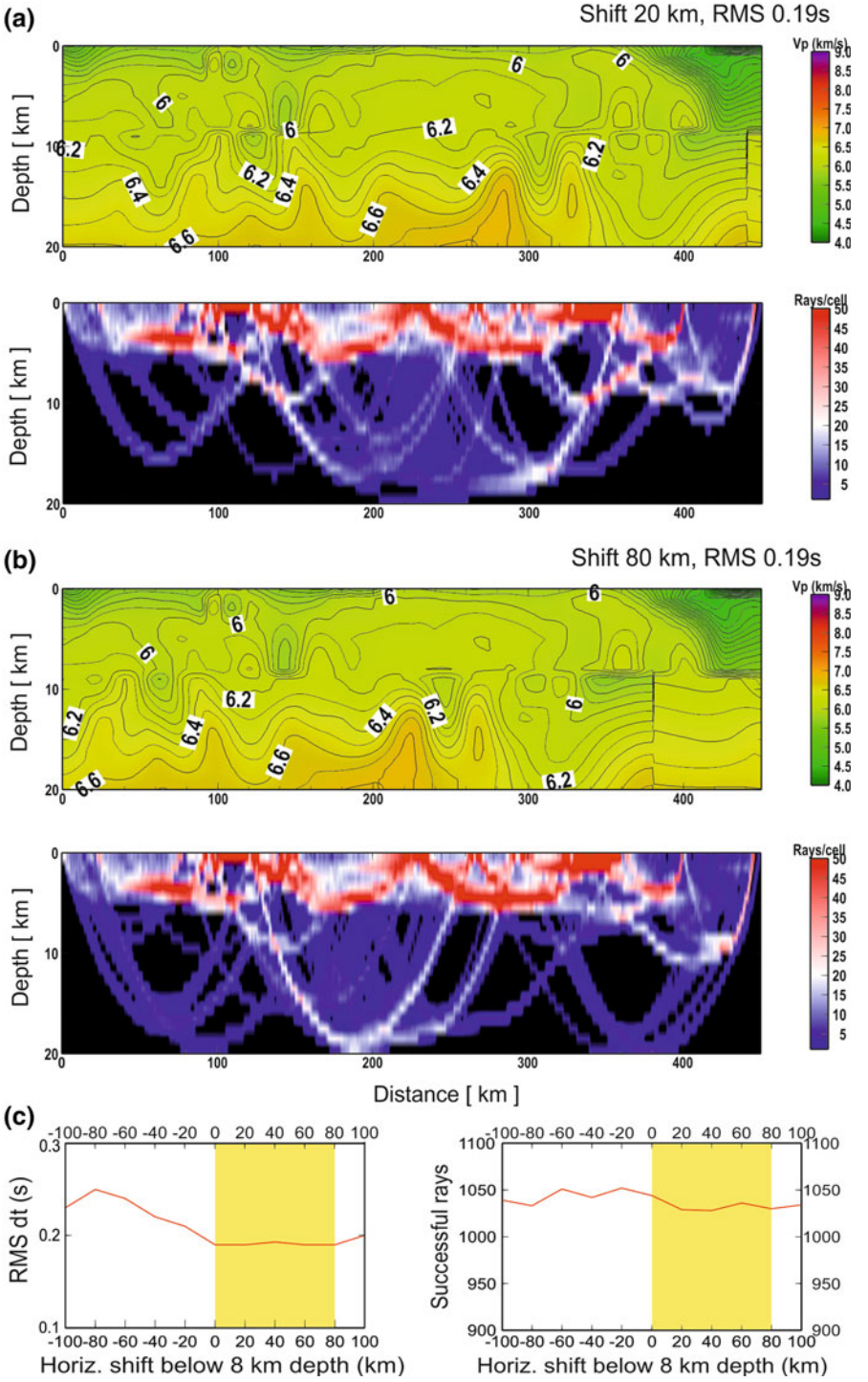
(a)
Shift 20 km, RMS 0.19s
Vp (km/s)
Depth [km]
Rays/cell
(b)
Shift 80 km, RMS 0.19s
Distance [km]
(c)
RMS dt (s)
Successful rays
Horiz. shift below 8 km depth (km)
Horiz. shift below 8 km depth (km)

◀ **Fig. 3** **a** CEL09 velocity model of Novotný (2011, Figure 10) with layers at depths of 9–20 km shifted by 20 km. **b** The same model shifted by 80 km. Both models have corresponding ray coverage. **c** Diagrams of the RMS residuals for different shifted layers at depths of 9–20 km; number of successful rays for models with shift. Note RMS residuals for both models of 0.19 s similar to the original model (0.19 s) while still keeping the same amount of successful rays traced through the models (see *yellow rectangle* in **c**)

5 Conclusions

To conclude, the application of the DRTG tomographic approach which substantially overestimates data constraints in large parts of the model results in producing artificial periodic velocity anomalies in the first-arrival DRTG models at depths below ~8 km. The ray tracing tests disclosed that the ray coverage at deeper parts of the models drops dramatically (compared to what is presented by the authors) and is not sufficient to reliably recover the structure. Velocity anomalies at these depths can be replaced either by a 1-D velocity distribution or shifted laterally by as much as 60–80 km without any significant change of the fit to the data (RMS traveltime residuals) compared to the published models. In such a case, a minimum-structure model should be adopted. For these reasons, detailed interpretation at depths below ~8 km results in geological/tectonic implications of unconstrained velocity anomalies, which it is not possible to accept.

References

Babuška V, Cara M (1991) Seismic anisotropy in the earth. Kluwer Acad Publishers, Dordrecht, p 217

Ernst WG, Maruyama S, Wallis S (1997) Buoyancy-driven, rapid exhumation of ultrahigh-pressure metamorphosed continental crust. Proc Natl Acad Sci USA 94:9532–9537

Grad M, Guterch A, Mazur S, Keller GR, Špičák A, Hrubcová P, Geissler WH (2008) Lithospheric structure of the Bohemian Massif and adjacent Variscan belt in central Europe based on profile S01 from the SUDETES 2003 experiment. J Geophys Res 113:B10304. doi:10.1029/2007JB005497

Hrubcová P, Środa P, Grad M, Geissler WH, Guterch A, Vozár J, Hegedűs E, Sudetes 2003 Working Group (2010) From the Variscan to the Alpine Orogeny: crustal structure of the Bohemian Massif and the Western Carpathians in the light of the SUDETES 2003 seismic data. Geophys J Int. doi:10.1111/j.1365-246X.2010.04766.x

Hrubcová P, Środa P, Špičák A, Guterch A, Grad M, Keller GR, Brückl E, Thybo H (2005) Crustal and uppermost mantle structure of the Bohemian Massif based on CELEBRATION 2000 data. J Geophys Res 110:B11305. doi:10.1029/2004JB003080

Hrubcová P, Środa P, CELEBRATION 2000 Working Group (2008) Crustal structure at the easternmost termination of the Variscan belt based on CELEBRATION 2000 and ALP 2002 data. Tectonophysics 460:55–75. doi:10.1016/j.tecto.2008.07.009

Rey P, Vanderhaeghe O, Teyssier C (2001) Gravitational collapse of the continental crust: definition, regimes and modes. Tectonophysics 342:435–449

Růžek B, Hrubcová P, Novotný M, Špičák A, Karousová O (2007) Inversion of travel times obtained during active seismic refraction experiments CELEBRATION 2000, ALP 2002 and SUDETES 2003. Stud Geophys Geod 51:141–166

Vidale JE (1990) Finite-difference calculation of travel-times in three dimensions. Geophysics 55:521–526

Zelt CA (1999) Modelling strategies and model assessment for wide-angle seismic traveltime data. Geophys J Int 139:183–204